Paleoceanography and Paleoclimatology

RESEARCH ARTICLE
10.1029/2019PA003599

Assessing the Spatial Origin of Meltwater Pulse 1A Using Oxygen-Isotope Fingerprinting

N. K. H. Yeung[1], L. Menviel[1], K. J. Meissner[1], and E. Sikes[2]

[1]Climate Change Research Centre, University of New South Wales and ARC Centre of Excellence for Climate Extremes, Sydney, New South Wales, Australia, [2]Institute of Marine and Coastal Sciences, State University of New Jersey, Rutgers, New Brunswick, NJ, USA

Key Points:
- Climate simulations with prognostic oxygen isotopes are integrated transiently, to constrain the spatial origin of Meltwater Pulse 1A
- Simulated $\delta^{18}O$ in a scenario with meltwater contribution from the Antarctic and NH ice sheets agrees best with paleoproxy data
- A meltwater pulse with a sole southern source cannot be ruled out

Correspondence to:
N. Yeung,
nicholas.yeung@unsw.edu.au

Citation:
Yeung, N. K.-H., Menviel, L., Meissner, K. J., & Sikes, E. L. (2019). Assessing the spatial origin of Meltwater Pulse 1A using oxygen-isotope fingerprinting. *Paleoceanography and Paleoclimatology*, *34*, 2031–2046. https://doi.org/10.1029/2019PA003599

Received 27 FEB 2019
Accepted 22 NOV 2019
Accepted article online 26 NOV 2019
Published online 13 DEC 2019

Abstract One of the major phases of sea level rise during the last deglaciation (~19–11 thousand years before present [ka BP]) is Meltwater Pulse-1A (MWP-1A; ~14.5 ka BP), when sea levels rose by 8.6 to 18 m in less than 400 years. Whether the meltwater originated from the partial disintegration of northern hemispheric ice sheets, from Antarctica, or both, remains controversial. Here we perform a series of idealized transient simulations of the last deglaciation, focusing on MWP-1A, with a three-dimensional oxygen-isotope enabled Earth System Climate Model. Three meltwater scenarios are considered during MWP-1A: a sole northern hemispheric source discharging into the North Atlantic, a sole Antarctic source, and a combined northern hemispheric-Antarctic source. A comparison of simulated changes in the oxygen-isotope composition ($\delta^{18}O$) of seawater and calcite with published marine sediment records points to a significant contribution from Antarctica. The best model-data fit is obtained with a contribution from both hemispheres. While the simulated changes over the 350 years of MWP-1A are overestimated in our simulations, the millennial-scale changes (~14.6–13 ka BP) are underestimated, potentially alluding to a longer and sustained meltwater input over the whole period. Meltwater was not applied in the Arctic, the Gulf of Mexico, or the North Pacific in our simulations, and therefore, scenarios with meltwater originating from these regions cannot be excluded.

1. Introduction

The last deglaciation (~19–10 ka BP) represents a major transition in Earth's climate, during which global temperatures increased by ~3.5 °C (Jouzel et al., 2007; Shakun et al., 2012) and atmospheric carbon dioxide concentration increased by ~95 ppmv (Monnin et al., 2001). The disintegration of northern hemispheric continental ice sheets, combined with Antarctic ice loss and thermal expansion, led to a global sea level rise of ~134 m (Lambeck et al., 2014).

During the early part of the last deglaciation, during Heinrich Stadial 1 (H1; ~17.5–14.7 ka BP), the formation of North Atlantic Deep Water (NADW) weakened significantly (Gherardi et al., 2005; McManus et al., 2004), thus maintaining cold conditions in the North Atlantic region and over Greenland (Buizert et al., 2014; Martrat et al., 2007), while the southern hemisphere warmed significantly (Denton et al., 2010; Parrenin et al., 2012). NADW strengthening at the end of H1 is associated with the Bølling-Allerød warm period (BA) (Buizert et al., 2014), while warming in Antarctica was interrupted by relatively cold conditions (Jouzel et al., 2007; Petit et al., 1999) during the Antarctic Cold Reversal (ACR; 14.7–13 ka BP). The ACR and the BA are in part an expression of the so-called bipolar seesaw effect (Broecker, 1998; Clark et al., 2012; Stocker & Johnsen, 2003), whereby warming in the northern hemisphere is accompanied by cooling at middle to high southern latitudes. It involves a strengthening of NADW formation, which increases the meridional heat transport to the North Atlantic (Crowley, 1992; Liu et al., 2009; Menviel et al., 2011). The warming from the BA could have caused excess loss from northern ice sheets. Previous modeling studies suggest that the amplitude of the southern cooling during the ACR could be explained with (Menviel et al., 2011; Weaver et al., 2003) or without (Pedro et al., 2016) meltwater input into the Southern Ocean.

Deschamps et al. (2012) refined the chronology of a major phase of sea level rise, known as Meltwater Pulse 1A (MWP-1A), and constrained its occurrence between 14.65 and 14.3 ka BP. With an estimated 8.6 to 18 m of sea level rise in less than 400 years (Deschamps et al., 2012; Liu et al., 2016), MWP-1A displayed the fastest rate of sea level rise during the last deglaciation (Bard et al., 1996; Hanebuth et al., 2000). The source and

spatial origin of the meltwater causing MWP-1A is still debated. Ackert et al., 2007, Licht (2004), and Mackintosh et al. (2011) argue that Antarctic ice sheets were unlikely to be the sole or even dominant source of meltwater, based on ice sheet constraints and modeling experiments. Gregoire et al. (2012),Gregoire et al. (2016) also support the hypothesis of a major meltwater source originating from North America, highlighting the possible disintegration of the Cordilleran-Laurentide ice saddle, which would have led to a global mean sea level rise of up to 6 m. Although the separation of the Cordilleran-Laurentide ice sheet simulated in Gregoire et al. (2016) occurs after 12 ka BP, possibly due to model biases, the authors suggest it might have taken place close to 14.6 ka BP, since meltwater contribution amplified by the BA provides the best match to geological data. However, by comparing sea level fingerprints, Clark et al. (2002) suggested that a sole southern Laurentide Ice Sheet source could not have been sufficient and thus supported a substantial meltwater contribution from the Antarctic ice sheets during MWP-1A. By forcing an Earth System model of intermediate complexity with meltwater fluxes into the Southern Ocean, Weaver et al. (2003) simulated a cooling at high southern latitudes and warming at high northern latitudes, with similarities to the onset of both BA and ACR. However, this northern warming caused by a meltwater contribution in the Southern Ocean is not replicated by all climate models. For example, in Stouffer et al. (2007), an Antarctic meltwater flux leads to a cooling in the North Atlantic instead, as convection is suppressed due to the spreading of low salinity waters to the north.

The occurrence of ice rafted debris in the South Atlantic at the time of MWP-1A (Weber et al., 2014) also lends support to an Antarctic contribution to MWP-1A. These phases of ice rafted debris discharges were contemporaneous with simulated Antarctic discharges (Golledge et al., 2014), which estimated an Antarctic ice sheet sea level equivalent (s.l.e.) contribution of ~2 m during the 350 years of MWP-1A and an additional 4 to 7.5 m between 15 and 13 ka BP. However, it is worth mentioning that the Antarctic disintegration simulated by Golledge et al. (2014) at the time of MWP-1A was due to a subsurface warming, which itself was obtained by adding a 5.3 m s.l.e into the Southern Ocean.

A review by Carlson and Clark (2012) suggests a total of 14 to 15 m of sea level rise during MWP-1A, with a northern contribution of 6.5 to 10 m, and a significant Antarctic contribution. A more recent study by Liu et al. (2016) indicates a global mean sea level rise of 8.6 to 14.6 m during MWP-1A (95% probability) but is unable to support or refute the possibility of a significant contribution from Antarctica.

The oxygen isotopic composition of seawater provides a useful tool to assess the spatial origin of MWP-1A. Owing to Rayleigh distillation during evaporation and precipitation, the oxygen isotopic composition

$$\delta^{18}\mathrm{O} = \left(\frac{\left({}^{18}\mathrm{O}/{}^{16}\mathrm{O}\right)_{\mathrm{sample}}}{\left({}^{18}\mathrm{O}/{}^{16}\mathrm{O}\right)_{\mathrm{standard}}} - 1 \right) \times 10^{3} \quad (1)$$

of continental ice sheets is significantly lower than that of seawater ($\delta^{18}O_w$). Consequently, extensive meltwater input would temporarily impact $\delta^{18}O_w$ close to the continental ice sheets of origin. To reconstruct past $\delta^{18}O_w$, $\delta^{18}O$ is often measured in the calcite shells of foraminifera ($\delta^{18}O_c$). $\delta^{18}O_c$ is a function of local seawater temperature and $\delta^{18}O_w$, with the latter being a function of ocean circulation, mixing, precipitation, evaporation, sea ice formation, and melting as well as discharge from land (rivers and ice sheet calving). The separation of $\delta^{18}O_c$ into its $\delta^{18}O_w$ and temperature components poses a major challenge in paleoceanography. While temperature can be estimated from a number of different techniques (e.g., Mg/Ca, $U^{k'}_{37}$, and foraminifera assemblages) so that a $\delta^{18}O_w$ signal can then be determined from $\delta^{18}O_c$, not all $\delta^{18}O_c$ records are associated with a temperature record, and some $\delta^{18}O_c$ records may not have a sufficient resolution to resolve the processes occurring at the time of MWP-1A.

Complementary information can be obtained by conducting simulations with oxygen-isotope-enabled climate models and then comparing the $\delta^{18}O_c$ signal calculated from simulated $\delta^{18}O_w$ and seawater temperature to the $\delta^{18}O_c$ record from marine sediment cores. Given that previous studies have highlighted the dominance of the temperature signal on benthic $\delta^{18}O$ (Bagniewski et al., 2015; Bagniewski et al., 2017; Zhang et al., 2017) and that there are significant uncertainties associated with changes in deep Atlantic Ocean temperatures, our model-data comparison focuses on the surface ocean.

Here, we use the UVic ESCM to conduct a series of transient simulations of the last deglaciation to investigate the origin of the meltwater that caused MWP-1A. Results of the simulations are compared with planktic $\delta^{18}O_c$ from the Atlantic and the Southern Oceans.

2. Methods

2.1. Model Description

The UVic ESCM, Version 2.9, is a fully coupled three-dimensional climate model of intermediate complexity, comprising atmosphere, land surface, vegetation, ocean, sea ice, and sediment components. The model is fully described by Weaver et al. (2001) and Meissner et al. (2003). The spherical grid resolution of UVic ESCM is 3.6° in longitude and 1.8° in latitude across all model components. UVic ESCM does not include flux adjustments, and water, energy, and carbon are conserved to numerical precision.

The ocean component of UVic ESCM is an ocean general circulation model with rigid-lid approximation (Pacanowski, 1995) that consists of 19 vertical levels, with a level thickness varying between 50 m at the surface and 500 m at 5 km depth. Mesoscale eddies are parameterized by the isopyncal diffusion scheme from Gent and McWilliams (1990). The atmospheric component is a vertically integrated two-dimensional energy and moisture balance model. It is forced by seasonally varying insolation and reanalysis winds from the National Center for Environmental Prediction (Kalnay et al., 1996), which are modified based on geostrophic adjustment due to air temperature anomalies (Weaver et al., 2001). The land components are the Met Office Surface Exchanges Scheme (MOSES) coupled to the dynamic global vegetation component TRIFFID (Top-down Representation of Interactive Foliage and Flora Including Dynamics) (Meissner et al., 2003). The UVic ESCM employs a standard thermodynamic-dynamic sea ice model (Hibler, 1979; Semtner, 1976), comprising subgridscale ice-covered and open-ocean categories, with elastic-viscous-plastic sea ice dynamics Hunke & Dukowicz, 1997 and a height-varying sea ice layer. Snow that falls on sea-ice may grow as a single height-varying snow layer.

The version of UVic ESCM that is used here includes oxygen isotopes (^{16}O and ^{18}O). These two stable isotopes are conserved in the model and incorporated in the atmosphere, ocean, land surface, and sea-ice components (Bagniewski et al., 2015; Bagniewski et al., 2017; Brennan et al., 2012; Brennan et al., 2013). They are exchanged across boundaries between the components, and fractionation is included during phase changes (Brennan et al., 2012).

The UVic ESCM represents the first-order changes in atmospheric $\delta^{18}O_w$ and compares well with observations and simulations with the NCAR CAM2 model under present-day boundary conditions (Brennan et al., 2012). However, changes in atmospheric dynamics are not well represented and might impact $\delta^{18}O_w$ in precipitation and therefore the ocean surface fluxes, but these changes are likely small in comparison to the changes induced by the depleted meltwater discharge and circulation changes.

2.2. Experimental Setup

Before the start of the transient simulations, the model was equilibrated for 11,000 model-years under constant (LGM) boundary conditions, including an orbital configuration corresponding to 21 ka BP (Berger, 1978), northern hemispheric ice sheet extent, topography and surface ice albedo at 21 ka BP (Peltier, 1994), an atmospheric carbon dioxide concentration of 189.65 ppm, and a global mean ocean $\delta^{18}O$ of 2‰.

Starting from the equilibrated state at 21 ka BP, the model is transiently integrated for 3,000 years to 18 ka BP under varying orbital parameters (Berger, 1978), carbon dioxide concentrations (Bereiter et al., 2012), and continental ice sheet geometry (Peltier, 1994). This sets the stage for the beginning of H1 (17.5–14.7 ka BP) during which we add a freshwater forcing of 0.075 Sv (1 Sv = $10^6 m^3 s^{-1}$) into the North Atlantic, with a $\delta^{18}O_w$ signature of −20‰ (Ferguson & Jasechko, 2015). This corresponds to the equivalent of approximately 20 m of sea level rise, in agreement with some paleoproxy reconstructions (Clark et al., 2009; Lambeck et al., 2014) and results in a weakening of NADW (McManus et al., 2004; Ng et al., 2018). To enable the recovery and overshoot of NADW (Liu et al., 2009) and therefore the transition to BA, a negative freshwater forcing of −0.2 Sv without a $\delta^{18}O$ signal (i.e., salt) is added to the same region of the North Atlantic between 15 and 14.65 ka BP.

We then perform four parallel transient simulations for the period between 14.65 and 13 ka BP. These simulations differ in the amount of freshwater forcing, the location at which this freshwater forcing is applied, and the $\delta^{18}O$ signal of the imposed freshwater fluxes. Details on the freshwater forcing applied in these simulations are shown in Table 1.

For MWP-1A (14.65–14.3 ka BP), three different meltwater scenarios are considered. All add 0.46 Sv of meltwater into the ocean over 350 years, which corresponds to 14 m s.l.e. In the first scenario (MWPfwNA), meltwater is only added into the North Atlantic (green box in Figure 2a). The second scenario (MWPfwSO)

Table 1
Freshwater Forcing and Its $\delta^{18}O_w$ Signature Used for Each of the Transient Simulations

	Simulation stage	H1	H1 recovery	MWP-1A					Recovery		Post-recovery
	Time (ka BP)	18–15	15–14.65	14.65–14.3					14.3–14.1		14.1–13
Freshwater flux	North Atlantic			48.6–63.0°N; 302.4–360.0°E							/
	Input (Sv)	0.075	−0.2	0.46	/	0.16	/	/	−0.3	−0.2	/
	$\delta^{18}O_w$ signal (‰)	−20	/	−20	/	−20	/	/	/	/	/
	Southern Ocean	/	/	82.8–63.0°S; 169.2–360.0°E					/		/
	Input (Sv)	/	/	/	0.46	0.3	/	/	/	/	/
	$\delta^{18}O_w$ signal (‰)	/	/	/	−36	−36	/	/	/	/	/
Sim. name	MWPfwNA	•	•	•					•		•
	MWPfwSO	•	•		•			•			•
	MWPfwC1	•	•			•				•	•
	noforcing	•	•				•	•			•

Note. H1 stands for Heinrich Stadial 1 and MWP-1A for Meltwater Pulse 1A. The locations of freshwater fluxes applied in MWP-1A are indicated in Figures 2a, 2d, and 2g.

involves a partial disintegration of the Antarctic ice sheet, where meltwater is added evenly across ocean grid boxes in the Ross Sea and Weddell Sea sector, as indicated in Figure 2d (red box). Finally, in the third scenario (MWPfwC1), the meltwater forcing is split between the North Atlantic (0.16 Sv) and the Ross Sea and Weddell Sea sector (0.3 Sv; green and red boxes in Figure 2g). This third scenario has a southern contribution of ~9 m s.l.e. The isotopic composition of the meltwater sources varies between hemispheres; while northern meltwater carries a $\delta^{18}O$ signal of −20‰ (Ferguson & Jasechko, 2015), southern meltwater is more depleted in our simulations with −36‰ (Grootes & Stuiver, 1997). At the end of the freshwater forcing, a salt flux is applied to the North Atlantic for simulations MWPfwNA and MWPfwC1, in order to enable NADW to recover (14.3–14.1 ka BP). The forcing is equivalent to −0.3 and −0.2 Sv in MWPfwNA and MWPfwC1, respectively. NADW does not shut down in MWPfwSO (Figure 1); hence, there is no need to apply a salt flux. After the recovery period, all simulations are integrated until 13 ka BP. A control simulation (noforcing), without any freshwater forcing after BA, is also integrated. All four simulations are transiently forced with changes in orbital parameters, carbon dioxide concentrations, and continental ice sheets. The control simulation therefore helps to attribute the impacts of the different meltwater scenarios.

2.3. Model-Data Comparison

The isotope-enabled UVic ESCM simulates $\delta^{18}O_w$, while paleoproxy archives from marine sediment cores record foraminiferal $\delta^{18}O_c$. Since $\delta^{18}O_c$ is temperature dependent, a temperature effect must be added to the simulated $\delta^{18}O_w$, in order to compare model simulations with paleoproxy records. Here, we use the equation derived by Shackleton (1974):

$$T = 16.9 - 4.38\left(\delta^{18}O_c - \delta^{18}O_w\right) + 0.10\left(\delta^{18}O_c - \delta^{18}O_w\right)^2. \quad (2)$$

If an ocean temperature record is available together with $\delta^{18}O_c$ data for a given marine sediment core or if there is an independent temperature record, the above equation can also be used to remove the temperature effect from the foraminiferal $\delta^{18}O_c$ record, to derive a $\delta^{18}O_w$ record that can be compared directly with the simulated $\delta^{18}O_w$.

Given that the simulations produced the most significant changes in the North Atlantic and Southern Oceans, comparisons are made in the South Atlantic, South Pacific, North Atlantic Oceans, and the Iberian Margin, where paleoproxy records of planktic $\delta^{18}O_c$ with sufficient resolution to resolve the period 15 to 13.5 ka BP are available. SST reconstructions from cores where planktic $\delta^{18}O_c$ has been measured are also included. Details of the paleoproxy records used in this study are listed in Table A1 in Appendix A.

3. Model Results

For all model simulations, freshwater forcing significantly affects the ocean circulation (Figure 1). Meltwater input into the North Atlantic during H1 reduces the surface density, thus leading to a collapse of NADW

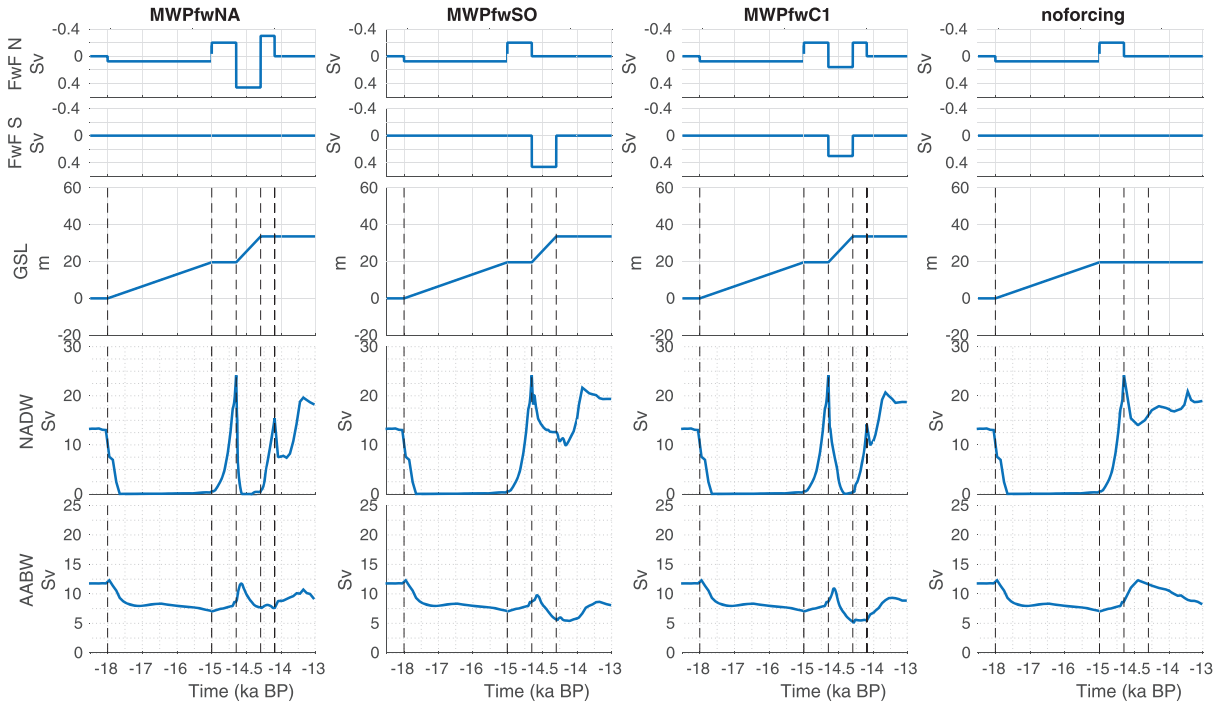

Figure 1. Time series of (from top to bottom) freshwater input into the North Atlantic (FwF N) and Southern Ocean (FwF S), corresponding global s.l.e. (sea level equivalent, GSL) only accounting for the meltwater input that carries a δ^{18}O signal, North Atlantic Deep Water (NADW), and Antarctic Bottom Water (AABW) transport. Each column represents a different experiment (from left to right): a sole northern hemispheric source (MWPfwNA), a sole Antarctic source (MWPfwSO), a combined northern hemispheric and Antarctic source (MWPfwC1), and a control run with no meltwater input during MWP-1A (noforcing). Note that the time axes are not linear, the time between 15 and 14 ka BP has been expanded by a factor of 3 for better readability during MWP-1A.

formation between 18 and 15 ka BP (Figure 1). Salt addition into the North Atlantic at the end of H1 leads to a resumption and overshoot (24 Sv) of NADW during the BA, as well as a slight strengthening of Antarctic Bottom Water (AABW) due to salt advection into the Southern Ocean. In the noforcing run, when no freshwater forcing is applied after the BA, NADW drops to ~15 Sv at ~14.5 ka BP and then slowly increases over the remaining 1,500 years of the simulations to ~19 Sv. At the same time, AABW strengthens, reaches ~12 Sv at ~14.5 ka BP, and then weakens linearly to ~8 Sv by 13 ka BP (Figure 1, right column, noforcing).

3.1. North Atlantic Meltwater Input

When meltwater is added into the North Atlantic during MWP-1A, it causes a rapid shutdown of NADW formation, while AABW weakens to ~8 Sv (Figure 1, left column, MWPfwNA). When the freshwater forcing is replaced by a salt flux at 14.3 ka BP, NADW recovers and reaches ~15 Sv. Similar to the simulation with a sole North Atlantic meltwater source (MWPfwNA, 0.46 Sv), meltwater addition into the North Atlantic (0.16 Sv) in the combined simulation (MWPfwC1) causes a NADW shutdown, albeit at a slower rate (Figure 1, third column). The subsequent recovery of NADW following MWP-1A is also similar to that produced in MWPfwNA.

The meltwater addition into the North Atlantic Ocean has a $\delta^{18}O_w$ signature of −20‰. The addition of depleted freshwater in combination with changes in ocean dynamics (Bagniewski et al., 2015) leads to a decrease in $\delta^{18}O_w$ of 2 to 4‰ at the surface of the North Atlantic in MWPfwNA (Figure 2a) and up to 1.8‰ in MWPfwC1 (Figure 2g). The ^{18}O-depleted surface water in MWPfwNA is carried into the South Atlantic by the northern subtropical gyre and the Brazil current, resulting in a surface water decrease of 0.6 to 1.2‰ in the South Atlantic. This signal also reaches intermediate depths and is seen in the top 1,000 m of the ocean (not shown).

The shutdown of NADW in both MWPfwNA and MWPfwC1 leads to a reduction in meridional heat transport, causing a decrease in sea surface temperature (SST) of over 5 °C in the North Atlantic (Figures 2c and 2i). A warming is simulated in the South Atlantic in MWPfwNA. Since a temperature decrease results in a

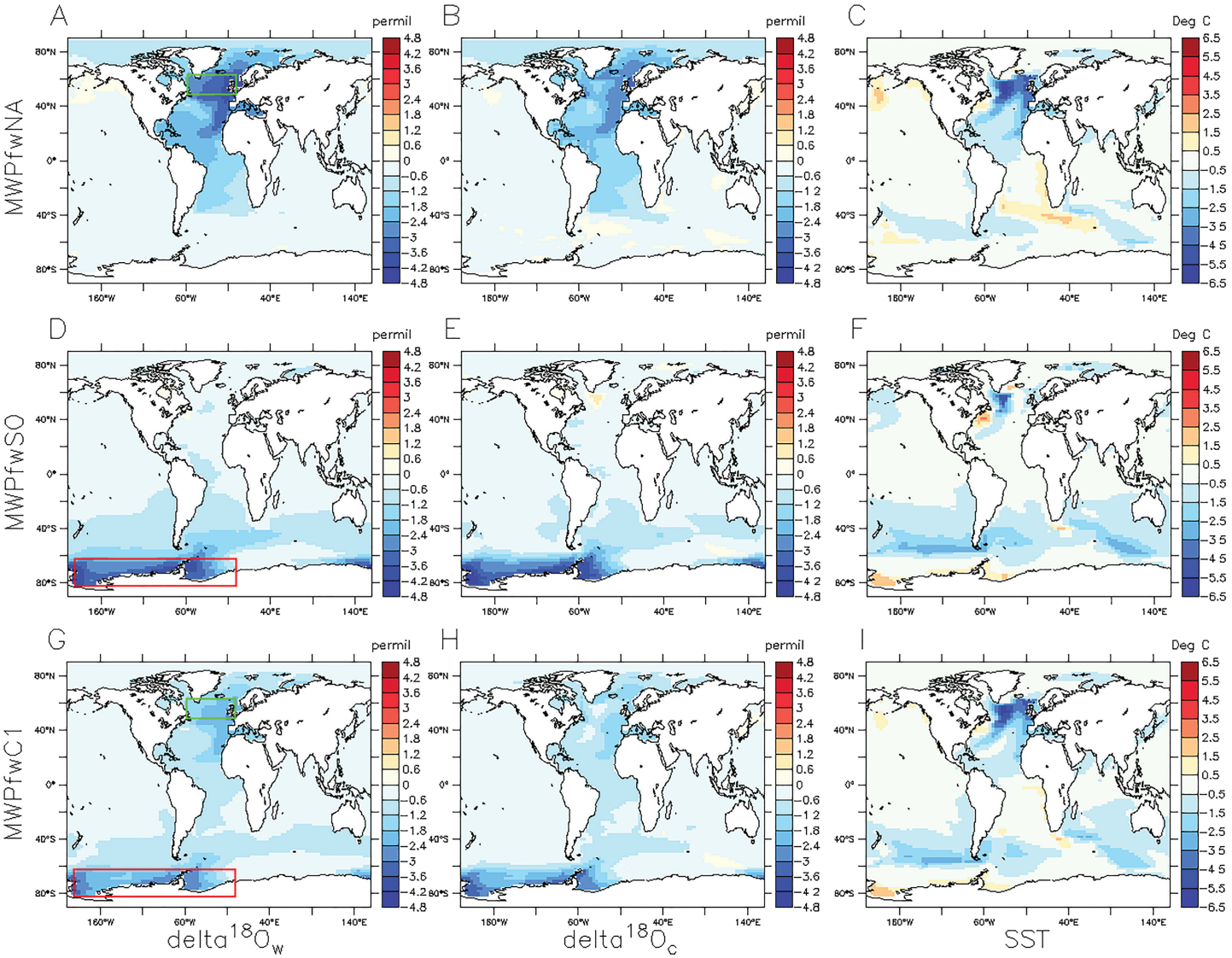

Figure 2. Surface anomalies as simulated in Experiments MWPfwNA (a–c), MWPfwSO (d–f), and MWPfwC1 (g–i) at 14.3 ka BP compared to 14.65 ka BP. (a,d,g) $\delta^{18}O_w$ (‰), (b,e,h) $\delta^{18}O_c$ (‰), and (c,f,i) SST (°C). The green and red boxes in (a), (d), and (g) indicate the areas where meltwater is added in the corresponding experiment.

$\delta^{18}O_c$ increase (equation (2)), the decrease in surface $\delta^{18}O_c$ during MWP-1A over the North Atlantic is not as prominent as in surface $\delta^{18}O_w$ (Figures 2a and 2b and 2g and 2h).

3.2. Southern Ocean Meltwater Input

In agreement with previous studies, meltwater addition to the Southern Ocean leads to increased stratification that reduces AABW formation from 10 to 6 Sv between 14.65 and 14.3 ka BP (Figure 1, second column) and decreases SSTs between 40°S and 60°S (Figure 2f). This increases the southern hemisphere sea ice extent (Menviel et al., 2010). However, in the region south of 60°S, SST increases by up to 1.8 °C in the Ross Sea (Figure 2f). NADW drops from over 24 Sv at the start of MWP-1A to ~13 Sv (Figure 1, second column). This decrease is largely due to the system readjusting after the overshoot during the BA, as a similar pattern is observed in noforcing (Figure 1, right column). Similar to MWPfwSO, meltwater addition into the Southern Ocean (0.3 Sv) in MWPfwC1 causes a weakening of AABW to 5 Sv.

Freshwater addition into the Southern Ocean with a $\delta^{18}O$ signature of −36‰, combined with associated changes in ocean dynamics, causes a $\delta^{18}O_w$ decrease of over 4‰ in the Southern Ocean in MWPfwSO (Figure 2d) and over 2.4‰ in MWPfwC1 (Figure 2g), particularly in the Ross and Weddell Sea sectors. Unlike

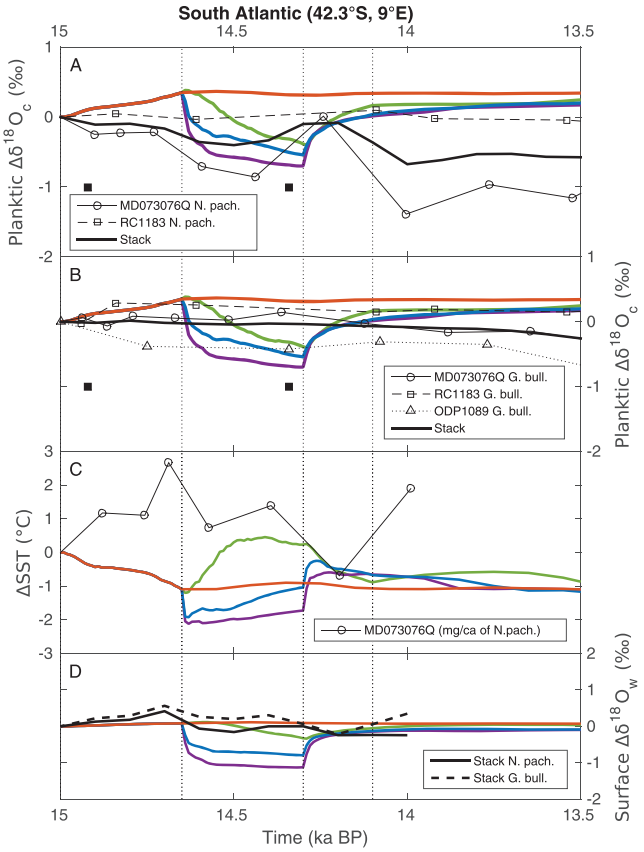

Figure 3. Time series of simulated surface $\delta^{18}O_c$ (a, b), SST (c), and $\delta^{18}O_w$ (s) anomalies (reference point taken at 15 ka BP) in the South Atlantic for experiments MWPfwNA (green), MWPfwSO (purple), MWPfwC1 (blue), and noforcing (orange), compared to planktic $\delta^{18}O_c$ data from two foraminifera species: *Neogloboquadrina pachyderma* (N. pach.) (a) and *Globigerina bulloides* (G. bull.) (b), from MD07-3076Q (Gottschalk et al., 2015), RC11-83 (Charles et al., 1996), and ODP1089 (Hodell et al., 2003). Solid squares in black represent the age tie points of RC11-83 (age tie point methods are listed in Appendix A). A $\delta^{18}O_c$ stack is inferred for both species. Estimates of change in $\delta^{18}O_w$ are derived from $\delta^{18}O_c$ stacks and SST record from MD07-3076Q (Riveiros et al., 2010).

in simulation MWPfwNA, where the $\delta^{18}O_w$ signal is advected into the Southern Hemisphere, the Southern Ocean freshwater signal largely remains south of 40°S (Figure 2d).

In MWPfwSO, a 4 °C cooling is simulated south of Greenland, while a 3 °C SST increase is simulated at ~40°N on the North American continental shelf (Figure 2f). This bipolar pattern is due to a weakening of the Gulf Stream and points to a shift in North Atlantic deep convection sites. The overall spatial distribution of changes in $\delta^{18}O_c$ (Figure 2e) is similar to $\delta^{18}O_w$ (Figure 2d), but $\delta^{18}O_c$ decreases less in the South Pacific as the SSTs over this region cool.

In general, spatial changes in surface $\delta^{18}O_w$, $\delta^{18}O_c$, and SSTs in MWPfwC1 (Figures 2g–2i) can be largely interpreted as a combination of the results obtained in MWPfwNA and MWPfwSO.

4. Model-Data Comparison

In this section, simulated changes in planktic $\delta^{18}O_c$, SSTs, and $\delta^{18}O_w$ between 15 and 13.5 ka BP are compared against a number of paleoproxy records from the South Atlantic, the South Pacific, the North Atlantic Oceans, and the Iberian Margin. In general, most SST and $\delta^{18}O_c$ records show good agreement with model results up to 15 ka BP. Due to uncertainties in constraining the timing of MWP-1A in proxies, model-data comparisons in Figure 5–8 share a reference point at 15 ka BP, in order to include any potential MWP-1A signal in the proxy data and better compare with model results.

4.1. South Atlantic Ocean

In the South Atlantic (Figure 3, 42.3°S, 9°E), the surface $\delta^{18}O_w$ in the control simulation (noforcing) remains stable throughout BA and MWP-1A, while MWPfwNA, MWPfwSO, and MWPfwC1 all experience a drop in surface $\delta^{18}O_w$ between 14.65 and 14.3 ka BP (Figure 3d). Due to the amount of ^{18}O-depleted meltwater added to the Southern Ocean, the signal is the strongest in MWPfwSO (Figure 3, purple), followed by MWPfwC1 (blue) and MWPfwNA (green). A decrease in surface $\delta^{18}O_w$ is also seen in the simulation forced with a sole northern hemispheric source (MWPfwNA), albeit to a lesser extent and with a greater time lag, since the low-$\delta^{18}O_w$ meltwater signal takes time to propagate southward from the North Atlantic and becomes diluted on its way.

Local SSTs in the South Atlantic (42.3°S, 9°E) increase by 1.5 °C for MWPfwNA and decrease by up to 1 °C for simulations including southern hemispheric meltwater sources (MWPfwSO and MWPfwC1; Figure 3c). Similar to the $\delta^{18}O_w$ response, the SST response in the South Atlantic due to northern-originated meltwater (MWPfwNA) is slower.

There is a divergence between the model and data from 15 ka BP because the model simulates a cooling while the proxy records a warming. This could be due to the simulated AMOC recovery occurring 200 years too early. In all simulations (except noforcing), the resulting $\delta^{18}O_c$ decreases in the South Atlantic (Figure 3a), in relative agreement with the *Neogloboquadrina pachyderma* (*N. pachyderma*) record of MD07-3076Q (Gottschalk et al., 2015), and ODP1089 (Hodell et al., 2003) *Globigerina bulloides* (*G. bulloides*; Figure 3b) record. However, no significant $\delta^{18}O_c$ changes are apparent in RC11-83 (Charles et al., 1996).

The magnitude of the simulated $\delta^{18}O_c$ decrease is ~1‰ in 350 years compared to 0.3 to 0.5‰ in 1,500 years in the records, but it should be noted that the forcing applied in these simulations is idealized both in time and space. Taking dating uncertainties into account and the spread across the proxy records, this data-model comparison in the South Atlantic does neither validate nor exclude any of the scenarios presented. However, the drop of 0.7‰ from 15 to 14.4 ka BP and 1.4‰ at ~14.2 ka BP in MD07-3076Q does favor the existence of a southern meltwater contribution.

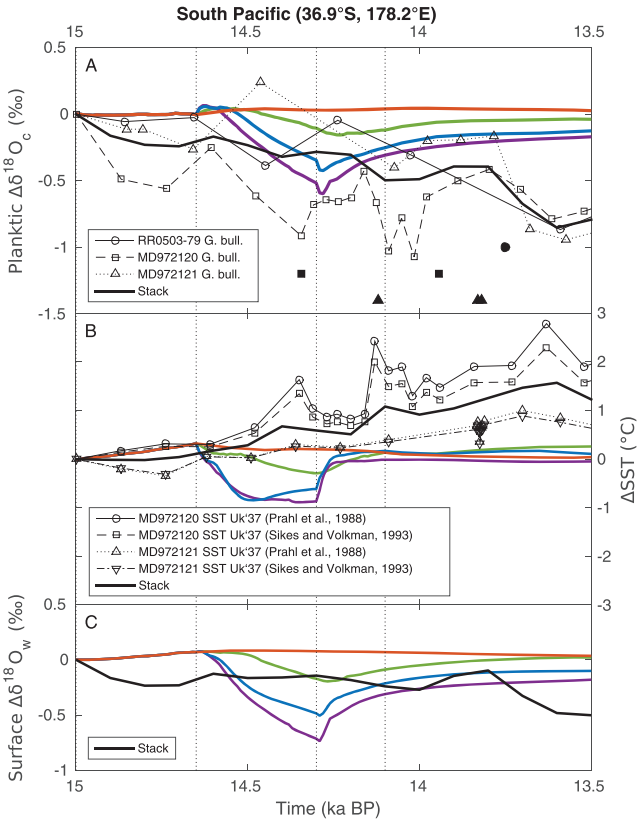

Figure 4. Time series of simulated surface $\delta^{18}O_c$ (a), SST (b) and $\delta^{18}O_w$ (c) anomalies (reference point taken at 15 ka BP) in the South Pacific for Experiments MWPfwNA (green), MWPfwSO (purple), MWPfwC1 (blue), and noforcing (orange), compared to planktic (*Globigerina bulloides*, G. bull.) $\delta^{18}O_c$ data from RR0503-79 (Schiraldi et al., 2014), MD97-2120 (Pahnke et al., 2003), and MD97-2121 (Carter et al., 2008). Solid symbols in black represent the age tie points of corresponding records (Appendix A). SST paleoproxy records from MD97-2120 and MD97-2121 (Pahnke and Sachs (2006), using calibration of Prahl et al. (1988) and Sikes and Volkman (1993)) are shown. $\delta^{18}O_c$ and SST stacks are generated from these cores and used to derive a $\delta^{18}O_w$ signal.

4.2. South Pacific Ocean

The time series of simulated $\delta^{18}O_w$ in the South Pacific (36.9°S, 178.2°E) (Figure 4) are similar to the ones in the South Atlantic, with all three meltwater simulations showing a significant decrease in $\delta^{18}O_w$. For MWPfwNA, SST decreases by ~0.5 °C in the South Pacific (Figure 4), unlike the warming simulated in the South Atlantic which amplifies the $\delta^{18}O_c$ decrease (Figure 3). As a result in the South Pacific, the $\delta^{18}O_c$ decrease in MWPfwNA is suppressed by the cooling SST.

The stack of SST reconstructions shows a long-term rising trend between 15 and 13.5 ka BP, which is not simulated in our experiments. However, the SST reconstruction of MD97-2120 does capture a similar short cooling from 14.4 to 14.2 ka BP as the one we simulate, though the simulated cooling occurs ~300 years earlier due to the timing of the forcing applied.

Planktic $\delta^{18}O_c$ records from the South Pacific display high variability from 15 to 13.5 ka BP. All $\delta^{18}O_c$ records, RR0503-79 (Schiraldi et al., 2014), MD97-2120 (Pahnke et al., 2003), and MD97-2121, (Pahnk & Sachs, 2006) show negative excursions of 0.5 to 0.8‰ at times and a long-term decrease of over 0.7‰ from 15 to 13.5 ka BP. The long-term $\delta^{18}O_c$ decrease is not simulated, partially due to a lack of long-term SST increase in our simulations, but also pointing to an addition of ^{18}O-depleted meltwater over a longer period as the $\delta^{18}O_w$ stack also suggests a long-term decrease of 0.5‰.

Given such high variability in the $\delta^{18}O_c$ records, it is difficult to reach a firm conclusion from our data-model comparison. However, MD97-2120 and to some extend RR0503-79 do display a $\delta^{18}O_c$ decrease of over 0.5‰ that would fit with the decrease simulated in MWPfwSO and MWPfwC1, indicating a potential southern meltwater source. Also, given that MWPfwSO and MWPfwC1 produce a $\delta^{18}O_c$ decrease that is over twice

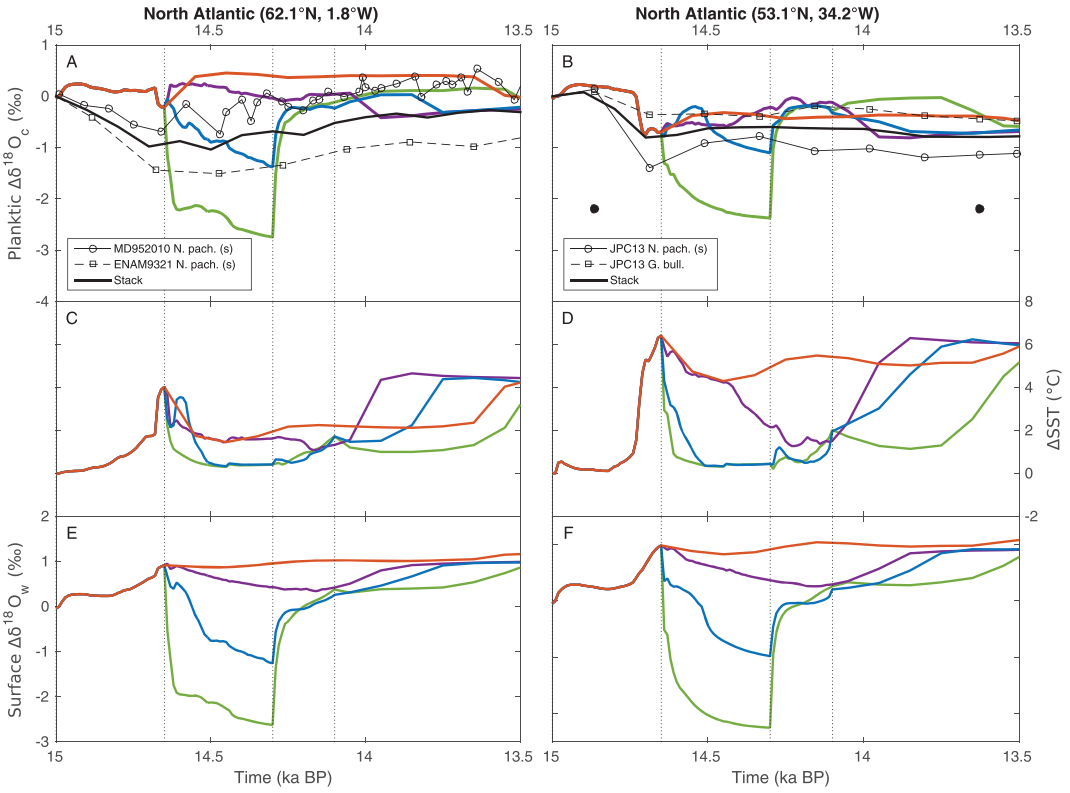

Figure 5. Time series of simulated surface $\delta^{18}O_c$ (a, b), SST (c, d), and $\delta^{18}O_w$ (e, f) anomalies (reference point taken at 15 ka BP) in the North Atlantic (left: 62.1°N, 1.8°W; right: 53.1°N, 34.2°W) for experiments MWPfwNA (green), MWPfwSO (purple), MWPfwC1 (blue), and noforcing (orange), compared to planktic $\delta^{18}O_c$ data from two foraminifera species: *Neogloboquadrina pachyderma* (N. pach.) and *Globigerina bulloides* (G. bull.), from MD95-2010 (Dokken & Jansen, 1999), ENAM93-21 (Rasmussen et al., 1996), and JPC-13 (Hodell et al., 2010). The solid circles in black represent the age tie points of JPC-13 (Appendix A). $\delta^{18}O_c$ stacks are shown for each species.

as large as the drop simulated in MWPfwNA, it suggests a sole NH meltwater source only leads to a small $\delta^{18}O_c$ decrease in the South Pacific. If the MWP-1A signal could be better isolated in the proxy record, the magnitude of $\delta^{18}O_c$ decrease could theoretically clearly identify a potential southern hemispheric meltwater source contribution.

4.3. North Atlantic Ocean

Simulated changes at two different locations in the North Atlantic (62.1°N, 1.8°W and 53.1°N, 34.2°W) are compared with sediment records in Figure 5. As expected, the largest surface $\delta^{18}O_w$ decrease (of up to 3.5‰) is simulated in the experiment with sole northern hemispheric meltwater forcing (MWPfwNA). In all simulations, an abrupt warming is simulated over Greenland and the North Atlantic during the BA due to the AMOC resumption following H1. The simulated peak warming occurs at 14.65 ka BP, which is potentially 100 to 200 years earlier than estimated from Greenland ice core records (Buizert et al., 2014), but within dating uncertainties. As NADW weakens in all simulations at the beginning of MWP-1A (Figure 1), a rather abrupt North Atlantic SST decrease is simulated. This cooling is more pronounced for simulations forced with freshwater in the North Atlantic (MWPfwNA and MWPfwC1), than in the control simulation and MWPfwSO. Even though this local cooling contributes to an increase in $\delta^{18}O_c$, the decrease in $\delta^{18}O_w$ due to the addition of ^{18}O-depleted meltwater dominates the signal in all simulations.

Simulated and $\delta^{18}O_c$ records in the North Atlantic largely agree before 15 ka BP (not shown), but they diverge starting from ~15 ka BP as a decrease in $\delta^{18}O_c$ is not simulated in the model between 15 and 14.7 ka BP (Figure 5a). This could imply a mismatch of MWP-1A timing of ~300 years. While the planktic $\delta^{18}O_c$ record of ENAM93-21 (Rasmussen et al., 1996) and JPC-13 (*G. bulloides*) (Hodell et al., 2010) do briefly show a drop of up to 1.5‰ in $\delta^{18}O_c$ (Figures 5a and 5b), the magnitude is much less than the drop simulated in

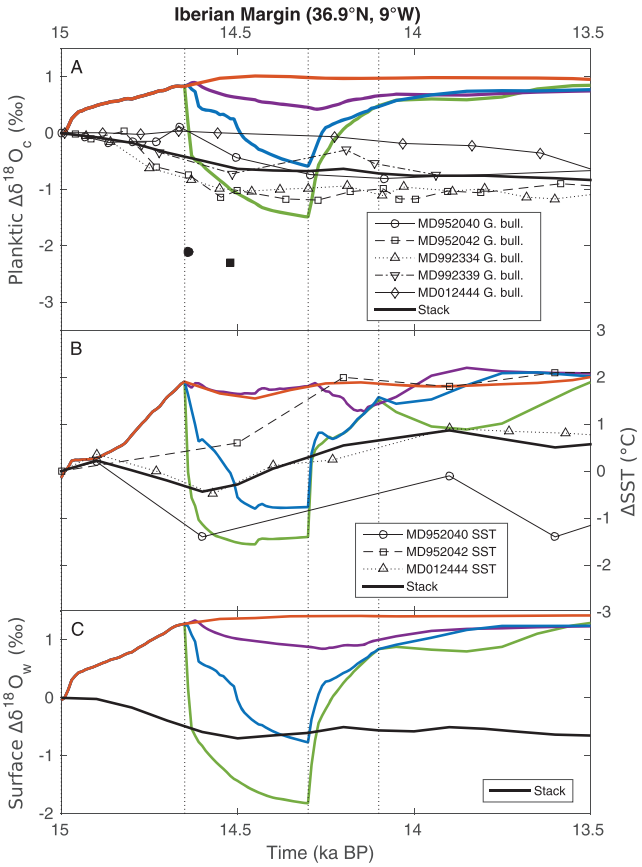

Figure 6. Time series of simulated surface $\delta^{18}O_c$ (a), SST (b), and $\delta^{18}O_w$ (c) anomalies (reference point taken at 18 ka BP) at the Iberian Margin for experiments MWPfwNA (green), MWPfwSO (purple), MWPfwC1 (blue), and noforcing (orange), compared to planktic $\delta^{18}O_c$ data from *Globigerina bulloides* (G. bull.), from MD95-2040 (Voelker & de Abreu, 2013), MD95-2042 (Shackleton et al., 2000), MD99-2334 (Skinner et al., 2003), MD99-2339 (Voelker et al., 2006), and MD01-2444 (Hodell et al., 2013). Solid symbols in black represent the age tie points of corresponding records (Appendix A). SST paleoproxy records from MD95-2040, MD95-2042 (Pailler & Bard, 2002), and MD01-2444 (Martrat et al., 2007) are shown. $\delta^{18}O_c$ and SST stacks are generated from these cores and used to derive a $\delta^{18}O_w$ signal.

MWPfwNA (green). As such, a case where significant southern meltwater is involved fits better with the paleoproxy records here.

4.4. Iberian Margin

The simulated time series of $\delta^{18}O_w$ and planktic $\delta^{18}O_c$ off the Iberian Margin (36.9°N, 9°W; Figure 6) are similar to those of the North Atlantic during MWP-1A (Figure 5). In simulations with northern hemispheric freshwater forcing, the NADW weakening leads to a SST decrease of ~3 °C (MWPfwNA and MWPfwC1). For simulations without meltwater forcing in the North Atlantic (noforcing and MWPfwSO), SSTs off the Iberian Margin do not experience a sharp drop during MWP-1A as was seen in the North Atlantic locations, implying that southern-originated meltwater forcing does not significantly affect SSTs at the Iberian Margin in our model (Figure 2f), in relative agreement with proxy records which do not show a significant cooling at this time. The greatest decrease in SST records shown in Figure 6b is ~1.5 °C, which is half of the decrease as simulated in MWPfwNA. Planktic $\delta^{18}O_c$ records from the Iberian Margin show a coherent trend (Figure 6a). They decrease by an average of 0.7‰ during the period from 15 to 14.3 ka BP, compared to a simulated reduction of over 2‰ in MWPfwNA and 0.5‰ and 1.5‰ in MWPfwSO and MWPfwC1, respectively, within 350 years. Similar to North Atlantic, simulated and planktic $\delta^{18}O_c$ records at the Iberian Margin generally agree before 15 ka BP (not shown), but there is a divergence afterward, possibly due to an earlier MWP-1A than simulated. Even when accounting for dating uncertainties, this is a strong indication that the decrease in $\delta^{18}O_w$ and SST is overestimated in our simulation with sole northern hemispheric freshwater forcing.

Comparison of simulated changes in $\delta^{18}O_c$ with existing planktic $\delta^{18}O_c$ records indicates that our simulated sole North American/ Eurasian meltwater source for MWP-1A is inconsistent with the available marine sediment data. Best agreement between the paleoproxy records and simulations are obtained for experiment MWPfwC1, which was forced with meltwater input into both the North Atlantic and Southern Ocean; while a sole southern source (MWPfwSO) cannot be ruled out.

5. Discussion

As meltwater from disintegrating continental ice sheets enters the ocean, it impacts the oxygen isotopic composition of the surrounding waters (Bagniewski et al., 2015) but also the large-scale oceanic circulation (Rahmstorf, 2002) and thus oceanic and atmospheric temperature and carbon reservoirs (Marcott et al., 2014). MWP-1A is a particularly important period of the last deglaciation, as sea levels rose by 8.6 to 18 m within a few centuries (Deschamps et al., 2012; Liu et al., 2016). However, the origin of the meltwater that was discharged during MWP-1A is still debated (Golledge et al., 2014; Gregoire et al., 2012; Gregoire et al., 2016; Ivanovic et al., 2018; Weber et al., 2014).

Ivanovic et al. (2018) recently suggested that the effects of a meltwater pulse into the North Atlantic would dominate the climatic response during MWP-1A, even if meltwater originating from Antarctic ice sheets would be twice its magnitude, thus making it difficult to detect a potential southern contribution by simply examining surface temperature change. Similar to Ivanovic et al. (2018) and other previous studies (Menviel et al., 2010; Swingedouw et al., 2009), our results suggest that a meltwater pulse into the Southern Ocean induces climatic changes that are often restricted to the southern hemisphere. This contrasts with North Atlantic meltwater pulses that have far-reaching climatic impacts (Kageyama et al., 2013; Stouffer et al., 2006). However, given that continental ice sheets have a significantly lower $\delta^{18}O$ content than seawater, changes in $\delta^{18}O_w$ can provide new insights into the origin of MWP-1A.

Here, we have investigated the temperature, $\delta^{18}O_w$, and $\delta^{18}O_c$ changes induced by meltwater pulses entering the North Atlantic, the Southern Ocean, and both combined and compared our results with marine sediment records. The amplitude of changes in surface $\delta^{18}O_w$ is closely linked to the proximity of the region of freshwater forcing: A North Atlantic meltwater pulse induces a significant $\delta^{18}O_w$ decrease at the surface of the North Atlantic, and a meltwater pulse originating from the Antarctic ice sheets induces a $\delta^{18}O_w$ decrease at the surface of the Southern Ocean. Even though a surface cooling is also simulated in the regions surrounding the freshwater forcing area, thus locally increasing $\delta^{18}O_c$, the $\delta^{18}O_w$ signal generally dominates the total response of $\delta^{18}O_c$ in our simulations leading to a local overall decrease.

The comparison of our model simulations with planktic $\delta^{18}O_c$ records from the North Atlantic (Figure 5) and Iberian Margin (Figure 6) suggests that most of the meltwater responsible for MWP-1A must have originated from Antarctic ice sheets. The planktic $\delta^{18}O_c$ records from the North Atlantic and Iberian Margin are fairly consistent over the period 15 to 13.5 ka BP, with stacks showing negative excursions of ~1‰. However, the simulated decrease in MWPfwNA is over twice as large and occurs over a much shorter period of time compared to $\delta^{18}O_c$ records. The drop in SST at the Iberian Margin in MWPfwNA (Figure 6) is also overestimated when compared to the brief decreases shown in SST reconstructions at 14.6 ka BP. In contrast, $\delta^{18}O_c$ records in the North Atlantic and at the Iberian Margin, and the derived $\delta^{18}O_w$ trend at the Iberian Margin fits much better with simulated scenarios where most of the meltwater originates from Antarctica (MWPfwSO and MWPfwC1).

Comparisons to the South Pacific records (Figure 4) support a potential southern meltwater source, while comparisons to the South Atlantic records (Figure 3) are relatively less conclusive. Though displaying considerable variability, planktic $\delta^{18}O_c$ data in the South Atlantic and South Pacific record an overall decreasing trend between 15 and 13.5 ka BP. In addition, some records do indicate fairly large (~0.6‰) and rapid $\delta^{18}O_c$ decreases between 14.6 and 14 ka BP, in agreement with a meltwater pulse into the Southern Ocean. However, the derived $\delta^{18}O_w$ signal from $\delta^{18}O_c$ records and SST reconstructions suggests the simulated $\delta^{18}O_w$ decrease in a southern-meltwater-only scenario (MWPfwSO) might be overestimated and points toward a scenario where at least some meltwater originated from northern hemispheric ice sheets. Another possibility is that meltwater originating from the Antarctic ice sheet was added over a longer period of time than simulated here.

Simulation MWPfwC1 mimics a scenario during which an equivalent of ~5 m sea level rise was added to the North Atlantic and an equivalent of ~9 m sea level rise to the Southern Ocean. In our experimental design, the freshwater forcing into the Southern Ocean was set to be greater than the North Atlantic contribution for two reasons: (i) to moderate the amplitude and slowdown the rate of NADW weakening (as opposed to the rapid shutdown simulated in MWPfwNA) and (ii) to obtain a clear $\delta^{18}O_w$ signal in the Southern Hemisphere.

Our model-data comparison in the North Atlantic supports a 0 to ~5 m s.l.e. contribution from the northern hemispheric ice sheet into the North Atlantic during MWP-1A, in agreement with previous ice sheet modeling studies, which suggest a 3 to 6 m contribution from the North American ice sheet (Gregoire et al., 2016). The Southern Ocean model-data comparison cannot provide quantitative estimates of the Antarctic ice sheet contribution but leans toward a scenario with a substantial contribution, of possibly 9 m or more.

In this study we did not assess a potential meltwater input into the Arctic, the Gulf of Mexico, or the North Pacific, even though there is some evidence of meltwater discharge into these regions. For example, paleoproxy records from the Gulf of Mexico have highlighted a significant $\delta^{18}O$ decrease surrounding the time of MWP-1A, thus suggesting that meltwater from the Laurentide ice sheet could have been routed toward the Gulf of Mexico instead of the North Altantic (Flower et al., 2004; Vetter et al., 2017). Planktic $\delta^{18}O_c$ records from the Gulf of Alaska and the northwest Pacific also indicate meltwater addition during the broad period of MWP-1A (Davies et al., 2011; Gorbarenko et al., 2019). Finally, meltwater input into the Arctic cannot be ruled out either (Poore et al., 1999).

While only a few records suggest a sharp $\delta^{18}O_c$ drop as seen in our simulations during the ~400 years of MWP-1A, the longer-term changes in the Southern Hemisphere are usually underestimated in our simulations, suggesting a continuous meltwater input over the period 14.6 to 13 ka BP. This model-data comparison thus indicates either that (i) the model is too sensitive to the meltwater input on centennial timescales; (ii) the paleoproxy records do not have the necessary resolution due to sedimentation rates or sampling interval to record the sharp change occurring during MWP-1A; (iii) the paleoproxy records are influenced by bioturbation or aliasing, such that if MWP-1A did produce a dramatic change in $\delta^{18}O_w$ or SST, the $\delta^{18}O_c$ record would have a less pronounced signal; (iv) meltwater was added to other regions, such as the Arctic (Poore et al., 1999), the Gulf of Mexico (Flower et al., 2004; Vetter et al., 2017), or the North Pacific; or (v) that meltwater was added over a longer time period.

The data-model comparison part of this study was limited by the number, resolution, and chronology of planktic $\delta^{18}O_c$ records available. Additional high-resolution records over the period of MWP-1A would be very valuable to improve our understanding of this important episode of fast sea level rise. Due to the general lack of carbonate sediments in the Southern Ocean, potential regions of interest include the midsouthern latitudes and the North Atlantic.

6. Conclusion

A suite of transient simulations of the last deglaciation was conducted with an oxygen-isotope enabled climate model to constrain the origin of the meltwater leading to the sea level rise during MWP-1A (~14.6–14.3 ka BP). Three meltwater scenarios were investigated: a sole northern hemispheric contribution added into the North Atlantic, a sole Antarctic contribution added into the Southern Ocean, and a combined contribution from the Laurentide and/or Eurasian ice sheets and Antarctic ice sheets. All scenarios lead to a significant weakening of NADW and AABW formation, thus impacting ocean temperatures. Simulated changes in oceanic seawater and calcite $\delta^{18}O$ ($\delta^{18}O_w$ and $\delta^{18}O_c$) were compared to a number of planktic $\delta^{18}O_c$ records from the South Atlantic, South Pacific, North Atlantic Oceans, and Iberian Margin.

The experiment with a sole northern source during MWP-1A is the least consistent with the paleoproxy data considered here. A combined source suggesting a disintegration of both the north hemispheric ice sheets and Antarctic ice sheets offers a better match, which is in broad agreement with recent studies suggesting a major Northern Hemisphere (Gregoire et al., 2016) and a moderate Antarctic origin (Golledge et al., 2014; Weber et al., 2014) of MWP-1A. A scenario with a sole southern source cannot be ruled out. Our experiments did not test other source regions and therefore do not exclude scenarios with meltwater input to the Arctic, the Gulf of Mexico, or the North Pacific. This study points to the need of additional high-resolution planktic $\delta^{18}O_c$ and SST records particularly in the Southern Ocean.

Paleoceanography

10.1029/2019PA003599

Table A1

Core location, tie points used for chronology, method used to derive the SST estimate and reference for all the marine records described in the study.

Core	Region	Latitude (°)	Longitude (°)	Depth (m)	Planktic species	Age tie point method	Reference	SST method	Reference
MD07-3076Q	South Atlantic	−44.15	−14.23	3,770	N. pach., G. bull.	/	Gottschalk et al. (2015)	Mg/Ca	Riveiros et al. (2010)
RC11-83	South Atlantic	−41.6	9.8	4,718	N. pach., G. bull.	Accelerator mass spectrometry (AMS) ^{14}C dates	Charles et al. (1996)	/	/
ODP1089	South Atlantic	−40.93	9.9	4,621	G. bull.	/	Hodell et al. (2003)	/	/
RR0503-79	South Pacific	−36.96	176.59	1,165	G. bull.	Tephra ages	Schiraldi et al. (2014)	/	/
MD97-2120	South Pacific	−45.53	174.93	1,210	G. bull.	AMS ^{14}C dates	Pahnke et al. (2003)	UK'_{37}	Pahnke and Sachs (2006)
MD97-2121	South Pacific	−40.37	177.98	3,014	G. bull.	AMS ^{14}C dates and tephra ages	Carter et al. (2008)	UK'_{37}	Pahnke and Sachs (2006)
MD95-2010	North Atlantic	66.68	4.57	1,226	N. pach.	/	Dokken and Jansen (1999)	/	/
ENAM93-21	North Atlantic	62.73	−4	1,020	N. pach.	/	Rasmussen et al. (1996)	/	/
JPC-13	North Atlantic	53.06	−33.52	3,082	G. bull., N. pach.	Correlating benthic δ^{18}O record to the benthic δ^{18}O record of core MD95-2042	Hodell et al. (2010)	/	/
MD95-2040	Iberian Margin	40.58	−9.86	2,465	G. bull.	End of termination IA in GISP2 according to de Abreu et al. (2003)	Voelker and de Abreu (2013)	UK'_{37}	Pailler and Bard (2002)
MD95-2042	Iberian Margin	37.8	−10.17	3,146	G. bull.	Correlating to the GRIP record	Shackleton et al. (2000)	UK'_{37}	Pailler and Bard (2002)
MD99-2334	Iberian Margin	37.8	−10.17	3,166	G. bull.	/	Skinner et al. (2003)	/	/
MD99-2339	Iberian Margin	35.89	−7.53	1,177	G. bull.	/	Voelker et al. (2006)	/	/
MD01-2444	Iberian Margin	37.57	−10.13	2,656	G. bull.	/	Hodell et al. (2013)	UK'_{37}	Martrat et al. (2007)

Note. N. pach. stands for *Neogloboquadrina pachyderma* and G. bull. for *Globigerina bulloides*.

Appendix A : Details of Planktic $\delta^{18}Oc$ and SST Records

Details the location, age model and reference of the d18Oc and SST records used in this study.

Acknowledgments
This research is the result of an Honours thesis that was funded through an honours scholarship scheme provided by the Australian Research Council's Centre of Excellence for Climate Extremes. Computational resources were provided by the NCI National Facility at the Australian National University, through awards under the Merit Allocation Scheme, the Intersect allocation scheme, and the UNSW HPC at NCI scheme. K. J. M., L. M., and N. Y. acknowledge support from the Australian Research Council (DP180100048, DE150100107, and FT180100606). The modeling data described in this study is published to Research Data Australia and can be accessed online (https://doi.org/10.26190/5d7ac7c4e8486).

References

de Abreu, L., Shackleton, N. J., Schönfeld, J., Hall, M., & Chapman, M. (2003). Millennial-scale oceanic climate variability off the western Iberian Margin during the last two glacial periods. *Marine Geology*, *196*(1-2), 1–20. https://doi.org/10.1016/S0025-3227(03)00046-X

Ackert, R. P. Jr., Mukhopadhyay, S., Parizek, B. R., & Borns, H. W. (2007). Ice elevation near the West Antarctic ce sheet divide during the last glaciation. *Geophysical Research Letters*, *34*, L21506. https://doi.org/10.1029/2007GL031412

Bagniewski, W., Meissner, K. J., & Menviel, L. (2017). Exploring the oxygen isotope fingerprint of Dansgaard-Oeschger variability and Heinrich events. *Quaternary Science Reviews*, *159*, 1–14. https://doi.org/10.1016/j.quascirev.2017.01.007

Bagniewski, W., Meissner, K. J., Menviel, L., & Brennan, C. E. (2015). Quantification of factors impacting seawater and calcite $\delta^{18}O$ during Heinrich Stadials 1 and 4. *Paleoceanography*, *30*(7), 895–911. https://doi.org/10.1002/2014PA002751

Bard, E., Hamelin, B., Arnold, M., Montaggioni, L., Cabioch, G., Faure, G., & Rougerie, F. (1996). Deglacial sea-level record from Tahiti corals and the timing of global meltwater discharge. *Nature*, *382*(6588), 241–244.

Bereiter, B., Lüthi, D., Siegrist, M., Schüpbach, S., Stocker, T. F., & Fischer, H. (2012). Mode change of millennial CO_2 variability during the last glacial cycle associated with a bipolar marine carbon seesaw. *Proceedings of the National Academy of Sciences of the United States of America*, *109*(25), 9755–9760. https://doi.org/10.1073/pnas.1204069109

Berger, A. (1978). Long-term variations of daily insolation and quaternary climatic changes. *Journal of the Atmospheric Sciences*, *35*(12), 2362–2367. https://doi.org/10.1175/1520-0469(1978)035<2362:LTVODI>2.0.CO;2

Brennan, C. E., Meissner, K. J., Eby, M., Hillaire-Marcel, C., & Weaver, A. J. (2013). Impact of sea ice variability on the oxygen isotope content of seawater under glacial and interglacial conditions. *Paleoceanography*, *28*(3), 388–400. https://doi.org/10.1002/palo.20036

Brennan, C. E., Weaver, A. J., Eby, M., & Meissner, K. J. (2012). Modelling oxygen isotopes in the University of Victoria Earth system climate model for pre-industrial and last glacial maximum conditions. *Atmosphere-Ocean*, *50*(4), 447–465. https://doi.org/10.1080/07055900.2012.707611

Broecker, W. S. (1998). Paleocean circulation during the last deglaciation: A bipolar seesaw. *Paleoceanography*, *13*(2), 119–121. https://doi.org/10.1029/97PA03707

Buizert, C., Gkinis, V., Severinghaus, J. P., He, F., Lecavalier, B. S., Kindler, P., et al. (2014). Greenland temperature response to climate forcing during the last deglaciation. *Science*, *345*(6201), 1177–1180. https://doi.org/10.1126/science.1254961

Carlson, A. E., & Clark, P. U. (2012). Ice sheet sources of sea level rise and freshwater discharge during the last deglaciation. *Reviews of Geophysics*, *50*, RG4007. https://doi.org/10.1029/2011RG000371

Carter, L., Manighetti, B., Ganssen, G., & Northcote, L. (2008). Southwest pacific modulation of abrupt climate change during the antarctic cold reversal–younger dryas. *Palaeogeography, Palaeoclimatology, Palaeoecology*, *260*(1), 284–298. https://doi.org/10.1016/j.palaeo.2007.08.013

Charles, C. D., Lynch-Stieglitz, J., Ninnemann, U. S., & Fairbanks, R. G. (1996). Climate connections between the hemisphere revealed by deep sea sediment core/ice core correlations. *Earth and Planetary Science Letters*, *142*(1), 19–27. https://doi.org/10.1016/0012-821X(96)00083-0

Clark, P. U., Dyke, A. S., Shakun, J. D., Carlson, A. E., Clark, J., Wohlfarth, B., et al. (2009). The last glacial maximum. *Science*, *325*(5941), 710–714. https://doi.org/10.1126/science.1172873

Clark, P. U., Mitrovica, J. X., Milne, G. A., & Tamisiea, M. E. (2002). Sea-level fingerprinting as a direct test for the source of global meltwater pulse 1A. *Science*, *295*(5564), 2438–2441. https://doi.org/10.1126/science.1068797

Clark, P. U., Shakun, J. D., Baker, P. A., Bartlein, P. J., Brewer, S., Brook, E., et al. (2012). Global climate evolution during the last deglaciation. *Proceedings of the National Academy of Sciences*, *109*(19), E1134–E1142. https://doi.org/10.1073/pnas.1116619109

Crowley, T. J. (1992). North Atlantic deep water cools the southern hemisphere. *Paleoceanography*, *7*(4), 489–497. https://doi.org/10.1029/92PA01058

Davies, M. H., Mix, A. C., Stoner, J. S., Addison, J. A., Jaeger, J., Finney, B., & Wiest, J. (2011). The deglacial transition on the southeastern Alaska Margin: Meltwater input, sea level rise, marine productivity, and sedimentary anoxia. *Paleoceanography*, *26*, PA2223. https://doi.org/10.1029/2010PA002051

Denton, G. H., Anderson, R. F., Toggweiler, J. R., Edwards, R. L., Schaefer, J. M., & Putnam, A. E. (2010). The last glacial termination. *Science*, *328*(5986), 1652–1656. https://doi.org/10.1126/science.1184119

Deschamps, P., Durand, N., Bard, E., Hamelin, B., Camoin, G., Thomas, A. L., et al. (2012). Ice-sheet collapse and sea-level rise at the Bølling warming 14,600 years ago. *Nature*, *483*(7391), 559–564.

Dokken, T. M., & Jansen, E. (1999). Rapid changes in the mechanism of ocean convection during the last glacial period. *Nature*, *401*, 458–461.

Ferguson, G., & Jasechko, S. (2015). The isotopic composition of the Laurentide Ice Sheet and fossil groundwater. *Geophysical Research Letters*, *42*, 4856–4861. https://doi.org/10.1002/2015GL064106

Flower, B. P., Hastings, D. W., Hill, H. W., & Quinn, T. M. (2004). Phasing of deglacial warming and Laurentide Ice Sheet meltwater in the Gulf of Mexico. *Geology*, *32*(7), 597–600. https://doi.org/10.1130/G20604.1

Gent, P. R., & McWilliams, J. C. (1990). Isopycnal mixing in ocean circulation models. *Journal of Physical Oceanography*, *20*(1), 150–155. https://doi.org/10.1175/1520-0485(1990)020<0150:IMIOCM>2.0.CO;2

Gherardi, J.-M., Labeyrie, L., McManus, J., Francois, R., Skinner, L., & Cortijo, E. (2005). Evidence from the Northeastern Atlantic basin for variability in the rate of the meridional overturning circulation through the last deglaciation. *Earth and Planetary Science Letters*, *240*(3), 710–723. https://doi.org/10.1016/j.epsl.2005.09.061

Golledge, N. R., Menviel, L., Carter, L., Fogwill, C. J., England, M. H., Cortese, G., & Levy, R. H. (2014). Antarctic contribution to meltwater pulse 1A from reduced Southern Ocean overturning. *Nature Communications*, *5*(5107). https://doi.org/10.1038/ncomms6107

Gorbarenko, S., Shi, X., Zou, J., Velivetskaya, T., Artemova, A., Liu, Y., et al. (2019). Evidence of meltwater pulses into the North Pacific over the last 20 ka due to the decay of Kamchatka Glaciers and Cordilleran Ice Sheet. *Global and Planetary Change*, *172*, 33–44. https://doi.org/10.1016/j.gloplacha.2018.09.014

Gottschalk, J., Skinner, L. C., & Waelbroeck, C. (2015). Contribution of seasonal sub-Antarctic surface water variability to millennial-scale changes in atmospheric CO_2 over the last deglaciation and Marine Isotope Stage 3. *Earth and Planetary Science Letters*, *411*, 87–99. https://doi.org/10.1016/j.epsl.2014.11.051

Gregoire, L. J., Otto-Bliesner, B., Valdes, P. J., & Ivanovic, R. (2016). Abrupt Bølling warming and ice saddle collapse contributions to the Meltwater Pulse 1a rapid sea level rise. *Geophysical Research Letters*, *43*, 9130–9137. https://doi.org/10.1002/2016GL070356

Gregoire, L. J., Payne, A. J., & Valdes, P. J. (2012). Deglacial rapid sea level rises caused by ice-sheet saddle collapses. *Nature*, *487*, 219–222. https://doi.org/10.1038/nature11257

Grootes, P. M., & Stuiver, M. (1997). Oxygen 18/16 variability in Greenland snow and ice with 10^{-3}- to 10^{5}-year time resolution. *Journal of Geophysical Research*, *102*(C12), 26,455–26,470. https://doi.org/10.1029/97JC00880

Hanebuth, T., Stattegger, K., & Grootes, P. M. (2000). Rapid flooding of the Sunda Shelf: A late-glacial sea-level record. *Science*, *288*(5468), 1033–1035. https://doi.org/10.1126/science.288.5468.1033

Hibler, W. D. (1979). A dynamic thermodynamic sea ice model. *Journal of Physical Oceanography*, *9*(4), 815–846. https://doi.org/10.1175/1520-0485(1979)009<0815:ADTSIM>2.0.CO;2

Hodell, D. A., Crowhurst, S., Skinner, L., Tzedakis, P. C., Margari, V., Channell, J. E. T., et al. (2013). Response of iberian margin sediments to orbital and suborbital forcing over the past 420 ka. *Paleoceanography*, *28*(1), 185–199. https://doi.org/10.1002/palo.20017

Hodell, D. A., Evans, H. F., Channell, J. E. T., & Curtis, J. H. (2010). Phase relationships of North Atlantic ice-rafted debris and surface-deep climate proxies during the last glacial period. *Quaternary Science Reviews*, *29*(27), 3875–3886. https://doi.org/10.1016/j.quascirev.2010.09.006

Hodell, D. A., Venz, K. A., Charles, C. D., & Ninnemann, U. S. (2003). Pleistocene vertical carbon isotope and carbonate gradients in the South Atlantic sector of the Southern Ocean. *Geochemistry, Geophysics, Geosystems*, *4*(1), 1–19. https://doi.org/10.1029/2002GC000367

Hunke, E. C., & Dukowicz, J. K. (1997). An elastic–viscous–plastic model for sea ice dynamics. *Journal of Physical Oceanography*, *27*(9), 1849–1867. https://doi.org/10.1175/1520-0485(1997)027<1849:AEVPMF>2.0.CO;2

Ivanovic, R. F., Gregoire, L. J., Wickert, A. D., & Burke, A. (2018). Climatic effect of Antarctic meltwater overwhelmed by concurrent northern hemispheric melt. *Geophysical Research Letters*, *45*, 5681–5689. https://doi.org/10.1029/2018GL077623

Jouzel, J., Masson-Delmotte, V., Cattani, O., Dreyfus, G., Falourd, S., Hoffmann, G., et al. (2007). Orbital and millennial antarctic climate variability over the past 800,000 years. *Science*, *317*(5839), 793–796. https://doi.org/10.1126/science.1141038

Kageyama, M., Merkel, U., Otto-Bliesner, B., Prange, M., Abe-Ouchi, A., Lohmann, G., et al. (2013). Climatic impacts of fresh water hosing under Last Glacial Maximum conditions: A multi-model study. *Climate of the Past*, *9*(2), 935–953. https://doi.org/10.5194/cp-9-935-2013

Kalnay, E., Kanamitsu, M., Kistler, R., Collins, W., Deaven, D., Gandin, L., et al. (1996). The NCEP/NCAR 40-year reanalysis project. *Bulletin of the American Meteorological Society*, *77*(3), 437–471. https://doi.org/10.1175/1520-0477(1996)077<0437:TNYRP>2.0.CO;2

Lambeck, K., Rouby, H., Purcell, A., Sun, Y., & Sambridge, M. (2014). Sea level and global ice volumes from the Last Glacial Maximum to the Holocene. *Proceedings of the National Academy of Sciences*, *111*(43), 15,296–15,303. https://doi.org/10.1073/pnas.1411762111

Licht, K. J. (2004). The Ross Sea's contribution to eustatic sea level during meltwater pulse 1A. *Sedimentary Geology*, *165*(3), 343–353. https://doi.org/10.1016/j.sedgeo.2003.11.020

Liu, J., Milne, G. A., Kopp, R. E., Clark, P. U., & Shennan, I. (2016). Sea-level constraints on the amplitude and source distribution of meltwater pulse 1a. *Nature Geoscience*, *9*, 130.

Liu, Z., Otto-Bliesner, B. L., He, F., Brady, E. C., Tomas, R., Clark, P. U., et al. (2009). Transient simulation of last deglaciation with a new mechanism for Bølling-Allerød warming. *Science*, *325*(5938), 310–314. https://doi.org/10.1126/science.1171041

Mackintosh, A., Golledge, N., Domack, E., Dunbar, R., Leventer, A., White, D., et al. (2011). Retreat of the east Antarctic ice sheet during the last glacial termination. *Nature Geoscience*, *4*, 195.

Marcott, S. A., Bauska, T. K., Buizert, C., Steig, E. J., Rosen, J. L., Cuffey, K. M., et al. (2014). Centennial-scale changes in the global carbon cycle during the last deglaciation. *Nature*, *514*, 616–619. https://doi.org/10.1038/nature13799

Martrat, B., Grimalt, J. O., Shackleton, N. J., de Abreu, L., Hutterli, M. A., & Stocker, T. F. (2007). Four climate cycles of recurring deep and surface water destabilizations on the Iberian Margin. *Science*, *317*(5837), 502–507. https://doi.org/10.1126/science.1139994

McManus, J. F., Francois, R., Gherardi, J. M., Keigwin, L. D., & Brown-Leger, S. (2004). Collapse and rapid resumption of Atlantic meridional circulation linked to deglacial climate changes. *Nature*, *428*(6985), 834–837. https://doi.org/10.1038/nature02494

Meissner, K. J., Weaver, A. J., Matthews, H. D., & Cox, P. M. (2003). The role of land surface dynamics in glacial inception: A study with the UVic Earth System Model. *Climate Dynamics*, *21*(7), 515–537. https://doi.org/10.1007/s00382-003-0352-2

Menviel, L., Timmermann, A., Timm, O. E., & Mouchet, A. (2010). Climate and biogeochemical response to a rapid melting of the West Antarctic Ice Sheet during interglacials and implications for future climate. *Paleoceanography*, *25*, PA4231. https://doi.org/10.1029/2009PA001892

Menviel, L., Timmermann, A., Timm, O. E., & Mouchet, A. (2011). Deconstructing the Last Glacial termination: The role of millennial and orbital-scale forcings. *Quaternary Science Reviews*, *30*(9), 1155–1172. https://doi.org/10.1016/j.quascirev.2011.02.005

Monnin, E., Indermühle, A., Dällenbach, A., Flückiger, J., Stauffer, B., Stocker, T. F., et al. (2001). Atmospheric CO_2 concentrations over the last glacial termination. *Science*, *291*(5501), 112–114. https://doi.org/10.1126/science.291.5501.112

Ng, H. C., Robinson, L. F., McManus, J. F., Mohamed, K. J., Jacobel, A. W., Ivanovic, R. F., et al. (2018). Coherent deglacial changes in western Atlantic Ocean circulation. *Nature Communications*, *9*(1), 2947. https://doi.org/10.1038/s41467-018-05312-3

Pacanowski, R. (1995), MOM 2, Documentation, User's Guide and Reference Manual, GFDL Ocean Group Technical Report.

Pahnke, K., & Sachs, J. P. (2006). Sea surface temperatures of southern midlatitudes 0–160 kyr B.P. *Paleoceanography*, *21*(2), PA2003. https://doi.org/10.1029/2005PA001191

Pahnke, K., Zahn, R., Elderfield, H., & Schulz, M. (2003). 340,000-year centennial-scale marine record of southern hemisphere climatic oscillation. *Science*, *301*(5635), 948–952. https://doi.org/10.1126/science.1084451

Pailler, D., & Bard, E. (2002). High frequency palaeoceanographic changes during the past 140 000 yr recorded by the organic matter in sediments of the iberian margin. *Palaeogeography, Palaeoclimatology, Palaeoecology*, *181*(4), 431–452. https://doi.org/10.1016/S0031-0182(01)00444-8

Parrenin, F., Petit, J.-R., Masson-Delmotte, V., Wolff, E., Basile-Doelsch, I., Jouzel, J., et al. (2012). Volcanic synchronisation between the EPICA Dome C and Vostok ice cores (Antarctica) 0-145 kyr BP. *Climate of the Past*, *8*(3), 1031–1045.

Pedro, J. B., Bostock, H. C., Bitz, C. M., He, F., Vandergoes, M. J., Steig, E. J., et al. (2016). The spatial extent and dynamics of the Antarctic Cold Reversal. *Nature Geoscience*, *9*(1), 51–55.

Peltier, W. R. (1994). Ice age paleotopography. *Science*, *265*(5169), 195–201. https://doi.org/10.1126/science.265.5169.195

Petit, J. R., Jouzel, J., Raynaud, D., Barkov, N. I., Barnola, J. M., Basile, I., et al. (1999). Climate and atmospheric history of the past 420,000 years from the Vostok ice core, Antarctica. *Nature*, *399*(6735), 429–436.

Poore, R. Z., Osterman, L., Curry, W. B., & Phillips, R. L. (1999). Late pleistocene and Holocene meltwater events in the Western Arctic Ocean. *Geology*, *27*(8), 759–762. https://doi.org/10.1130/0091-7613(1999)027<0759:LPAHME>2.3.CO;2

Prahl, F. G., Muehlhausen, L. A., & Zahnle, D. L. (1988). Further evaluation of long-chain alkenones as indicators of paleoceanographic conditions. *Geochimica et Cosmochimica Acta*, *52*(9), 2303–2310. https://doi.org/10.1016/0016-7037(88)90132-9

Rahmstorf, S. (2002). Ocean circulation and climate during the past 120,000 years. *Nature*, *419*, 207–214. https://doi.org/10.1038/nature01090;

Rasmussen, T. L., Thomsen, E., Labeyrie, L., & van Weering, T. C. (1996). Circulation changes in the Faeroe-Shetland Channel correlating with cold events during the last glacial period (58-10 ka). *Geology*, *24*(10), 937–940.

Riveiros, N. V., Waelbroeck, C., Skinner, L., Roche, D. M., Duplessy, J.-C., & Michel, E. (2010). Response of south Atlantic deep waters to deglacial warming during Terminations V and I. *Earth and Planetary Science Letters*, *298*(3), 323–333. https://doi.org/10.1016/j.epsl.2010.08.003

Schiraldi, B., Sikes, E. L., Elmore, A. C., Cook, M. S., & Rose, K. A. (2014). Southwest Pacific subtropics responded to last deglacial warming with changes in shallow water sources. *Paleoceanography*, *29*(6), 595–611. https://doi.org/10.1002/2013PA002584

Semtner, A. J. (1976). A model for the thermodynamic growth of sea ice in numerical investigations of climate. *Journal of Physical Oceanography*, *6*(3), 379–389. https://doi.org/10.1175/1520-0485(1976)006<0379:AMFTTG>2.0.CO;2

Shackleton, N. J. (1974). Attainment of isotopic equilibrium between ocean water and the benthonic foraminifera genus Uvigerina: Isotopic changes in the ocean during the last glacial. *219*, 203–210.

Shackleton, N. J., Hall, M. A., & Vincent, E. (2000). Phase relationships between millennial-scale events 64,000–24,000 years ago. *Paleoceanography*, *15*(6), 565–569. https://doi.org/10.1029/2000PA000513

Shakun, J. D., Clark, P. U., He, F., Marcott, S. A., Mix, A. C., Liu, Z., et al. (2012). Global warming preceded by increasing carbon dioxide concentrations during the last deglaciation. *Nature*, *484*(7392), 49–54. https://doi.org/10.1038/nature10915

Sikes, E. L., & Volkman, J. K. (1993). Calibration of alkenone unsaturation ratios (Uk'37) for paleotemperature estimation in cold polar waters. *Geochimica et Cosmochimica Acta*, *57*(8), 1883–1889. https://doi.org/10.1016/0016-7037(93)90120-L

Skinner, L. C., Shackleton, N. J., & Elderfield, H. (2003). Millennial-scale variability of deep-water temperature and $\delta^{18}O_w$ indicating deep-water source variations in the Northeast Atlantic, 0–34 cal. ka BP. *Geochemistry, Geophysics, Geosystems*, *4*(12), 1098. https://doi.org/10.1029/2003GC000585

Stocker, T. F., & Johnsen, S. J. (2003). A minimum thermodynamic model for the bipolar seesaw. *Paleoceanography*, *18*(4), 1087. https://doi.org/10.1029/2003PA000920

Stouffer, R. J., Seidov, D., & Haupt, B. J. (2007). Climate response to external sources of freshwater: North Atlantic versus the Southern Ocean. *Journal of Climate*, *20*(3), 436–448. https://doi.org/10.1175/JCLI4015.1

Stouffer, R. J., Yin, J., Gregory, J. M., Dixon, K. W., Spelman, M. J., Hurlin, W., et al. (2006). Investigating the causes of the response of the thermohaline circulation to past and future climate changes. *Journal of Climate*, *19*(8), 1365–1387. https://doi.org/10.1175/JCLI3689.1

Swingedouw, D., Mignot, J., Braconnot, P., Mosquet, E., Kageyama, M., & Alkama, R. (2009). Impact of freshwater release in the North Atlantic under different climate conditions in an OAGCM. *Journal of Climate*, *22*(23), 6377–6403. https://doi.org/10.1175/2009JCLI3028.1

Vetter, L., Spero, H. J., Eggins, S. M., Williams, C., & Flower, B. P. (2017). Oxygen isotope geochemistry of Laurentide ice-sheet meltwater across Termination I. *Quaternary Science Reviews*, *178*, 102–117. https://doi.org/10.1016/j.quascirev.2017.10.007

Voelker, A. H. L., & de Abreu, L. (2013). A review of abrupt climate change events in the Northeastern Atlantic Ocean (Iberian Margin): Latitudinal, longitudinal, and vertical gradients. In H. Rashid, L. Polyak, & E. Mosley-Thompson (Eds.), *Abrupt Climate Change: Mechanisms, Patterns, and Impacts* (pp. 15–37). American Geophysical Union (AGU). https://doi.org/10.1029/2010GM001021

Voelker, A. H. L., Lebreiro, S. M., Schönfeld, J., Cacho, I., Erlenkeuser, H., & Abrantes, F. (2006). Mediterranean outflow strengthening during northern hemisphere coolings: A salt source for the glacial Atlantic. *Earth and Planetary Science Letters*, *245*(1), 39–55. https://doi.org/10.1016/j.epsl.2006.03.014

Weaver, A. J., Eby, M., Wiebe, E. C., Bitz, C. M., Duffy, P. B., Ewen, T. L., et al. (2001). The UVic Earth system climate model: Model description, climatology, and applications to past, present and future climates. *Atmosphere-Ocean*, *39*(4), 361–428. https://doi.org/10.1080/07055900.2001.9649686

Weaver, A. J., Saenko, O. A., Clark, P. U., & Mitrovica, J. X. (2003). Meltwater pulse 1A from Antarctica as a trigger of the Bølling-Allerød warm interval. *Science*, *299*(5613), 1709–1713. https://doi.org/10.1126/science.1081002

Weber, M. E., Clark, P. U., Kuhn, G., Timmermann, A., Sprenk, D., Gladstone, R., et al. (2014). Millennial-scale variability in Antarctic ice-sheet discharge during the last deglaciation. *Nature*, *510*, 134–138.

Zhang, J., Liu, Z., Brady, E. C., Oppo, D. W., Clark, P. U., Jahn, A., et al. (2017). Asynchronous warming and δ_{18}o evolution of deep Atlantic water masses during the last deglaciation. *Proceedings of the National Academy of Sciences*, *114*(42), 11,075–11,080. https://doi.org/10.1073/pnas.1704512114